JOURNAL OF AIRCRAFT
Vol. 42, No. 1, January–February 2005

# Influence of Angle of Attack and Stabilizer Deflection on T Empennage Flutter

V. D. Chuban*
*TsAGI, 140180, Zhukorsky, Russia*

**It was found using wind-tunnel tests of airplanes with T empennage that the critical speed of antisymmetric flutter (based on composition of bending and torsional oscillations of the vertical tail) has an abnormally strong dependence on stabilizer deflections and angle of attack. This specific kind of antisymmetric flutter is characterized by relatively large amplitudes of oscillations of the stabilizer in its plane. Additional work of the induced drag forces on the in-plane component of oscillations might explain the nature of this kind of flutter. The numerical method for flutter analysis is described, which takes into account the effect of angles of attack and sideslip and aerodynamic control angles on flutter critical parameters. The method is based on a modification of the vortex lattice method and allows for induced drag when computing generalized aerodynamic forces. Numerical results for the flutter critical speed compare well with test data for a dynamically similar model of the civil airplane T-shaped empennage.**

## Introduction

MANY types of airliners include a T-shaped empennage. Beginning in 1960, the Russian aviation industry designed several passenger and transport airplanes with T empennage. Practically from the very beginning, it was found that this airplane scheme has some negative features. One of the problems was related to the T-empennage design stage when satisfying the flutter requirements. It was found (in wind-tunnel tests) that the critical speed of antisymmetric flutter (based on the composition of the bending and torsional oscillations of the vertical tail) has an abnormally strong dependence on stabilizer deflections and angle of attack.[1]

Traditional numerical methods of flutter evaluation failed to predict the critical parameters of this kind of flutter. At the same time, all other kinds of T-empennage flutter (both symmetric and antisymmetric) showed proper correspondence between numerical and experimental results of critical speeds.

This specific kind of antisymmetric flutter is characterized by relatively large amplitudes of oscillations of the stabilizer in the $X$ direction (where the $X$ axis is oriented to the fuselage nose) in comparison with other kinds of T-empennage flutter. It was supposed that the additional work of the $X$ component of the induced drag on the $X$ component of oscillatory displacements might explain the nature of this kind of flutter. A method to take into account this particular feature is developed and described in this paper.

There are two approaches to numerical evaluation of flutter critical parameters, based on quasi-steady aerodynamics or unsteady aerodynamics. In its nature, flutter study is the stability analysis of the body motion when a combination of inertial, elastic, structural damping, and aerodynamic forces acts on the body. Usually, critical parameters of flutter, calculated by both approaches, are different. Typically (but not always), unsteady aerodynamics increases the critical speed and reduces the critical frequency. The numerical method described in the paper uses the quasi-steady aerodynamics. The method may be generalized to use unsteady aerodynamics.

Traditional approaches described in Refs. 2–4 to calculate aerodynamic forces in flutter rely on linearization of the aerodynamic forces in the domain of low angle of attack and principally fail to describe the dependence of flutter critical parameters on airplane angle of attack and/or controls setting angles.

The goal of the present paper is to provide a method capable of analyzing airplane flutter within nonseparated flow theory. A vortex-lattice method modification is used as the basis, which allows for induced drag. The theory is developed by introducing the notion of linearization point. The linearization point is defined as the airplane flow problem solution in the case where controls deflections are known, angle of attack and sideslip are nonzero, and infinitesimal displacements due to small elastic oscillations are added.

This approach takes into account 1) changes in no-penetration boundary conditions due to finite variation of normal vectors when finite values of angle of attack, sideslip, and controls setting are introduced and 2) linearization of expressions for the aerodynamic forces applied to the airplane that are involved in small elastic oscillations. The allowance for induced-drag, which is quadratic in its essence and adds terms to aerodynamic forces in the course of the linearization, is of importance.

## Vortex Lattice Method

Consider a thin load-carrying surface (Fig. 1). Let us assume that it is curvilinear and features a curvilinear partitioning into quadrilateral panels. The surface is placed in a quasi-steady nonseparated compressible inviscid (potential) flow whose freestream velocity is $\boldsymbol{V}_\infty$ (with the module $U_\infty$):

$$\boldsymbol{V}_\infty = U_\infty \begin{bmatrix} -\cos\alpha\cos\beta \\ \sin\alpha\cos\beta \\ -\sin\beta \end{bmatrix} \tag{1}$$

where $\alpha$ is the angle of attack and $\beta$ is the sideslip angle. Each side (edge) of the panels may be assumed to be a straight-line segment. Let us introduce at the center of an $i$th panel the collocation point $P_i$ and the normal vector $\boldsymbol{n}_i$. Each panel is associated with a vortex frame that is composed of four vortex segments with identical intensity $G_i$. The system of vortex frames ensures circulation-free flow around the surface.

Quasi-steady flow with circulation may be obtained by complementing the trailing edge with semi-infinite vortex frames with intensities $\boldsymbol{G}_{Wi}$ that are equal to intensities $G_i$ of the frames neighboring the trailing edge. Lateral edges (or whiskers) of the semi-infinite frames may be assumed to run along the freestream velocity vector $\boldsymbol{V}_\infty$. The set of semi-infinite frames forms the vortex sheet that sheds from the trailing edge. The system of conditions $G_{Wi} = G_i$ for the sheet frames ensures meeting the Zhukovsky–Kutta condition for the trailing edge.

The vector $\boldsymbol{G} = [G_1, G_2, \ldots, G_N]^T$ (where $N$ is the total number of panels) comprises unknown intensities $G_i$, which could be

Received 29 July 2003; revision received 18 January 2004; accepted for publication 10 February 2004. 

*Head, Department of Computational Structural Mechanics, Moscow Region; chuban_v@mtu-net.ru.

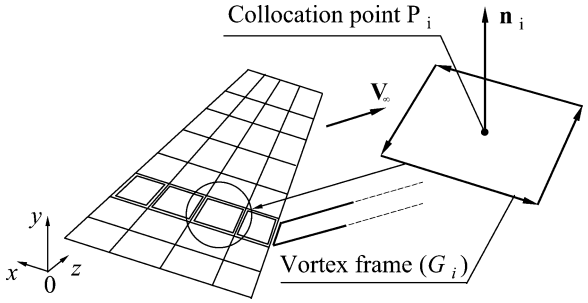


**Fig. 1 Discrete vortex frames on a load-carrying surface.**

determined by meeting $N$ no-penetration conditions for the set of collocation points $P_i$.

The approach to forming the discrete vortex system is rather equivalent to classical formulations of the vortex lattice method (VLM) and doublet lattice method (DLM). However, it has some special features. The features are as follows.

1) Instead of Eq. (1), both VLM and DLM usually rely on a simplified linearized expression.

2) The initial surface curvature and finite values of $\alpha$ and $\beta$ in these methods are usually taken into account by introducing infinitesimally small rotation of normal vectors in no-penetration conditions.

An $i$th vortex frame induces at a space point $P$ the velocity $V^{\text{ind}}(P) = V_i^{\text{ind}}(P)\boldsymbol{G}_i$, which may be computed via the velocity induced by each of the four segments of the frame (refer to Ref. 3). Note that the effect of the vortex frame adjacent to the trailing edge should be complemented with the velocity induced by the adjacent frame in the vortex sheet. The velocity induced by the surface itself and the vortex sheet could be written as

$$V^{\text{ind}}(P) = \sum_{i=1}^{N} V_i^{\text{ind}}(P)\boldsymbol{G}_i \tag{2}$$

Let us assume the surface displacement field at the point $P$ to be known,

$$U(P,t) = U^0(P) + u(P,t)$$

where $U^0$ is the stationary finite displacement caused, for example, by initial deflection of controls and/or static structural deformation; $u$ is the unsteady infinitesimal displacement of the surface point. With the displacement field known, we can also derive the surface velocity field,

$$V(P,t) = \dot{u}(P,t) \tag{3}$$

and the normal vectors,

$$\boldsymbol{n}(P,t) = \boldsymbol{n}^0(P) + \boldsymbol{\varphi}(P,t) \times \boldsymbol{n}^0(P) \tag{4}$$

where $\boldsymbol{n}^0$ is the normal vector with correction for surface displacement $U^0$ and $\boldsymbol{\varphi}$ is the infinitesimal rotation vector of the surface, associated with displacements $u$.

No-penetration conditions for the collocation point $P_j$ may be expressed as

$$\begin{aligned} \left[V_\infty + V^{\text{ind}}(P_j) - V\right] \cdot \boldsymbol{n}_j &= 0 \\ \boldsymbol{n}_j = \boldsymbol{n}(P_j,t), \qquad j &= 1,\ldots,N \end{aligned} \tag{5}$$

Substitute (2) – (4) and remove second-order terms to transform the conditions (5) into,

$$\sum_{i=1}^{N} A_{ji}\boldsymbol{G}_i = \boldsymbol{B}_j^0 + \boldsymbol{B}_j^v + \boldsymbol{B}_j^\varphi, \qquad j = 1,\ldots,N \tag{6}$$

where $A_{ji} = V_i^{\text{ind}}(P_j) \cdot \boldsymbol{n}^0(P_j)$ is the aerodynamic influence matrix coefficient. $\boldsymbol{B}_j^0 = -V_\infty \cdot \boldsymbol{n}_0(P_j)$, $\boldsymbol{B}_j^v = \dot{u}(P_j,t) \cdot \boldsymbol{n}_0(P_j)$, and $\boldsymbol{B}_j^\varphi = -V_\infty \cdot [\boldsymbol{\varphi}(P_j,t) \times \boldsymbol{n}_0(P_j)]$ are right-hand-side vector components. Equations (6) may be written by using matrix notation,

$$A\boldsymbol{G} = B^0 + B^v + B^\varphi \tag{7}$$

The solution to linear equation (7) can be decomposed as

$$\boldsymbol{G} = \boldsymbol{G}^0 + \boldsymbol{G}^v + \boldsymbol{G}^\varphi \tag{8}$$

Vector $\boldsymbol{G}^0$ is defined by vector $\boldsymbol{B}^0$ and characterizes vortex frame intensities as functions of angle of attack and sideslip and finite stationary displacements $U^0$. Vector $\boldsymbol{G}^v(t)$ is defined by vector $\boldsymbol{B}^v$ and characterizes vortex frame intensities as functions of velocities $\dot{u}$ of infinitesimal displacements. Vector $\boldsymbol{G}^\varphi(t)$ is defined by vector $\boldsymbol{B}^\varphi$ and characterizes vortex frame intensities as functions of surface rotation during infinitesimal displacements.

## Generalized Aerodynamic Forces

To compute force $F$ applied to a vortex segment, one can resort to Zhukovsky formula

$$F = \rho V \times \boldsymbol{\Gamma}\ell \tag{9}$$

in which $\rho$ is gas mass density, $V$ flow velocity at the vortex segment center, $\boldsymbol{\Gamma}$ vortex segment intensity vector, and $\ell$ vortex segment length. Note that vortex frame elements coinciding with the trailing edge, as well as vortex sheet elements, provide no contribution to aerodynamic forces.

With formula (9), the aerodynamic force acting on the vortex segment may be written as

$$F_k = F(R_k) = \rho\left[V_\infty + V^{\text{ind}}(R_k,t) - \dot{u}(R_k,t)\right] \times \boldsymbol{L}_k\boldsymbol{G}_k \tag{10}$$

where $R_k$ is the vortex segment center and $\boldsymbol{L}_k$ is the vortex segment vector. For the latter, we have

$$\boldsymbol{L}_k = \boldsymbol{L}_k^0 + \boldsymbol{\varphi}(R_k,t) \times \boldsymbol{L}_k^0 \tag{11}$$

which reflects variation of the vortex segment arrangement due to rotation during infinitesimal displacements.

Substitute Eqs. (2), (8), and (11) into Eqs. (10) and neglect second-order terms to derive the expression for the force applied to the vortex segment:

$$F_k = F_k^{00} + F_k^{0v} + F_k^{0\varphi} + F_k^{v0} + F_k^{\varphi 0}$$

where

$$F_k^{00} = \rho\left[V_\infty + \sum_{i=1}^{N} V_i^{\text{ind}}(R_k)\boldsymbol{G}_i^0\right] \times \boldsymbol{L}_k^0\boldsymbol{G}_k^0$$

$$F_k^{0v} = \rho\left[V_\infty + \sum_{i=1}^{N} V_i^{\text{ind}}(R_k)\boldsymbol{G}_i^0\right] \times \boldsymbol{L}_k^0\boldsymbol{G}_k^v$$

$$F_k^{0\varphi} = \rho\left[V_\infty + \sum_{i=1}^{N} V_i^{\text{ind}}(R_k)\boldsymbol{G}_i^0\right] \times \boldsymbol{L}_k^0\boldsymbol{G}_k^\varphi$$

$$F_k^{v0} = \rho\left[\sum_{i=1}^{N} V_i^{\text{ind}}(R_k)G_i^v - \dot{u}(R_k)\right] \times \boldsymbol{L}_k^0\boldsymbol{G}_k^0$$

$$F_k^{\varphi 0} = \rho\left\{\left[\sum_{i=1}^{N} V_i^{\text{ind}}(R_k)\boldsymbol{G}_i^\varphi\right] \times \boldsymbol{L}_k^0 + V_\infty \times \left[\varphi(R_k,t) \times \boldsymbol{L}_k^0\right]\right\}\boldsymbol{G}_k^0 \tag{12}$$

Relations (12) may be described in the following way:

$F_k^{00}$ is the stationary force depending only on angles of attack and sideslip and steady-state finite displacements of the surface.

$F_k^{0v}$ and $F_k^{v0}$ are unsteady forces depending on angle of attack and sideslip and steady-state displacements and are proportional to velocities of infinitesimal displacements.

$F_k^{0\varphi}$ and $F_k^{\varphi 0}$ are unsteady forces depending on angle of attack and sideslip and steady-state displacements and are proportional to rotation angles due to infinitesimal displacements.

Note that relations (12) are inherently quadratic because they comprise products of vortex frame intensities, so that the relations may be regarded as linearized approximations for aerodynamic forces, including induced drag. Relations (12) could be utilized in the usual way to compute generalized aerodynamic coefficients for equations of motion of an elastic structure placed in gas flow and involved in infinitesimal oscillations.

## Motion Equations for Elastic Structure

Consider an elastic structure with thin load-carrying surfaces. Its finite element model features positively definite and symmetric matrices of stiffness, $\mathcal{K}$, and mass, $\mathcal{M}$. Now the generalized eigenvalue/eigenvector problem should be solved:

$$\mathcal{K}\Phi_m = \omega_m^2 \mathcal{M}\Phi_m, \qquad m = 1, \ldots, M \tag{13}$$

(where $\Phi_m$ is an $m$th natural oscillation shape, $\omega_m$ is the angular frequency for the $m$th mode, and $M$ is the total number of modes) to obtain the basis for representing the displacement field of the structure (and its carrying surfaces):

$$u(P,t) = \sum_{m=1}^{M} \Phi_m(P) \cdot q_m(t) \tag{14}$$

The natural modes meet orthogonality and norming conditions,

$$\Phi_k^T \mathcal{M}\Phi_m = \delta_{km}, \qquad \Phi_k^T \mathcal{K}\Phi_m = \omega_m^2 \delta_{km} \tag{15}$$

By utilizing Eqs. (13–15) we derive equations for small elastic oscillations in the form[5]

$$\ddot{q}_m + 2\varsigma_m \omega_m \dot{q}_m + \omega_m^2 q_m = C_{q_m}^0 + \sum_{p=1}^{M} \left( C_{q_m}^{q_p} q_p + C_{q_m}^{\dot{q}_p} \dot{q}_p \right)$$
$$m = 1, \ldots, M \tag{16}$$

where $\varsigma_m$ is the structural damping coefficient for the $m$th mode.

Expressions for generalized aerodynamic coefficients present in the right-hand side of Eq. (16) are obtained from relations (12), (14), and (15). Note that the coefficients depend on angle of attack and sideslip, steady-state displacements $U^0$, and freestream speed $U_\infty$.

## Static Aeroelasticity

Small displacements of a structure placed in flow and not involved in oscillations meet the system

$$\omega_m^2 q_m = C_{q_m}^0 + \sum_{p=1}^{M} C_{q_m}^{q_p} q_p, \qquad m = 1, \ldots, M \tag{17}$$

which is obtained from Eq. (16) by neglecting terms with temporal derivatives. Let us assume that angles of attack and sideslip and initial steady-state displacements $U^0$ are known. One could arrange an iterative process for determining the equilibrium condition of the structure in flow:

1) On the basis of $\alpha$, $\beta$, and $U^0$, find generalized aerodynamic coefficients present in the right-hand side of algebraic equations (17).

2) Solve system (17) to obtain generalized amplitudes $q_m$.

3) Add the displacement field $u$ to $U^0$: $U^0 := U^0 + u$.

4) If the process converges (that is, generalized amplitudes are rather low), then the iterations are stopped.

5) Otherwise, stages 1–5 are repeated.

Note that if dynamic pressure is lower than the critical value able to result in structural divergence, then the process converges; usually, it suffices to run some 10 iterations.

Note that the main result from the procedure is the set of refined values of generalized aerodynamic coefficients for Eq. (16). In addition, coefficients $C_{q_m}^0$ tend to 0 during the process.

## Flutter

Flutter equations are obtained from Eq. (16) by removing the term $C_{q_m}^0$,

$$\ddot{\boldsymbol{q}}_m + 2\varsigma_m \omega_m \dot{\boldsymbol{q}}_m + \omega_m^2 \boldsymbol{q}_m = \sum_{p=1}^{M} \left( C_{q_m}^{q_p} q_p + C_{q_m}^{\dot{q}_p} \dot{q}_p \right)$$
$$m = 1, \ldots, M \tag{18}$$

The solution has the form $\boldsymbol{q}_m = \boldsymbol{q}_m e^{st}$, where $s = \sigma + i\omega$ is the complex angular frequency. With this, we derive the homogeneous algebraic system with real coefficients,

$$s^2 \boldsymbol{q}_m + 2s\varsigma_m \omega_m \boldsymbol{q}_m + \omega_m^2 \boldsymbol{q}_m = \sum_{p=1}^{M} \left( C_{q_m}^{q_p} q_p + sC_{q_m}^{\dot{q}_p} q_p \right)$$
$$m = 1, \ldots, M \tag{19}$$

By varying the flow velocity $U_\infty$, one can find purely imaginary values $s = i\omega$ that turn the system determinant into zero. The respective $\omega$ values define the flutter frequency, and a nontrivial vector $\boldsymbol{q}_m$ defines the structure flutter shape. In practical analysis the flutter equation (19) is easily solved by HQR algorithms (QR algorithms suggested by Francis and Kublanovskaja with preliminary Householder-transformation of matrix to Heissenberg-form).

## Results

Ability of the method is exemplified here by antisymmetric flutter of a dynamically similar model (DSM) of the civil airplane T-shaped empennage (Fig. 2). This model was comprehensively evaluated at SibNIA (Novosibirsk, Russia) to outline the influence of various factors on flutter critical parameter. Wind-tunnel tests were carried out at flow velocities of up to 45 m/s.

The DSM is symmetric relative to the (vertical) $0xy$ plane and includes six units: vertical stabilizer, rudder, left-hand and right-hand halves of the horizontal stabilizer, and left-hand and right-hand elevators. The rudder has four attachment points: The point second from the bottom features a spring that simulates an actuator. The elevator has seven attachment points: the point third from the vertical tail features a spring that simulates an actuator. Each of the units is made as a rectilinear aluminum spar with rigid sections attached.

The mathematical model computation included a beam-based finite element structural model and an aerodynamic model (Fig. 2). Results of modal analysis are compared with experimental data in Tables 1–3.

Modal tests were carried out in 1976 by using an obsolete concept as compared with state-of-the-art concepts. Oscillations were excited by utilizing rubber strips; this concept may turn out to overestimate oscillation frequency. Such circumstances should be taken into account when comparing data in Tables 1–3. Proceeding from

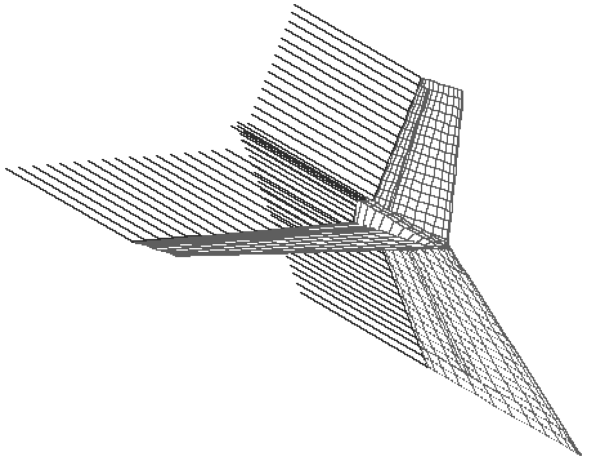

**Fig. 2 Aerodynamic model at stabilizer setting angle $\varphi_{st} = 12$ deg for T-shaped DSM; also vortex sheet whiskers.**

**Table 1 Natural frequencies of symmetric oscillations**

| Frequency $f$, Hz | | |
|---|---|---|
| Experiments | Theory | Description |
| 1.97 | 1.83 | Oscillations of vertical tail, chord plane |
| 3.78 | 2.56 | Horizontal oscillations of stabilizer, first mode |
| 5.08 | 4.42 | Bending of stabilizer, first mode |
| —— | 10.3 | Horizontal oscillations of stabilizer, second mode |
| —— | 11.5 | Bending of stabilizer, second mode |
| 12.3 | 11.9 | Torsion of stabilizer |

**Table 2 Natural frequencies of antisymmetric oscillations**

| Frequency $f$, Hz | | |
|---|---|---|
| Experiments | Theory | Description |
| 0.87 (0.9) | 0.916 | Bending of vertical tail, first mode |
| 1.85 (1.4) | 1.46 | Torsion of vertical tail |
| 3.23 | 3.18 | Bending of vertical tail, second mode |
| —— | 7.48 | Horizontal oscillations of stabilizer |
| 8.08 | 8.83 | Bending of stabilizer |
| 12.6 | 11.8 | Torsion of stabilizer |

**Table 3 Natural frequencies of elevator torsion in symmetric oscillations**

| Frequency $f$, Hz | | |
|---|---|---|
| Experiments | Theory | Description |
| 18.75 | 18.4 | Torsion of elevator at zero frequency of elevator rotation |
| 19.8 | 19.2 | Torsion of elevator at elevator rotation frequency of 10.55 Hz |

these same considerations, the tester team measured the first two frequencies of the antisymmetric spectrum while exciting the structure by hand. The frequencies thus obtained are shown in parentheses in the first two lines of Table 2. One can see good convergence of theoretical and experimental data.

The goals of the flutter tests included obtaining experimental dependence of the critical speed of antisymmetric flutter (with bending and torsion of the vertical tail) on angle of attack and stabilizer setting angle.

Angle of attack $\alpha$ was varied by rotating the entire structure in the vertical-tail chord plane. The stabilizer setting angle $\varphi_{st}$ was changed by turning the stabilizer around the $0z$ axis (normal to the symmetry plane $0xy$). During tests, the structure deformed notably; static vertical displacements of stabilizer tips were as large as 200 mm due to aeroelasticity.

Figures 3 and 4 show results of computing elastic rotation angle $\varphi_z$ for flow cross sections of the stabilizer and elevator at various stabilizer setting angles for flow velocity of 25.5 m/s. Clearly, flow changes structural geometry due to aeroelasticity. Note that at $\varphi_{st} = 12$ deg the theoretical vertical displacement of stabilizer tips is 216 mm, close to the earlier experimental data.

Figure 5 shows theoretical and experimental dependence of the flutter critical speed on angle of attack and stabilizer setting angle. The calculation did not allow for the influence of elasticity on structural geometry. It is clear that theoretical results are below the experimental ones.

Figure 6 shows the similar kind of dependence with the provision for elasticity, as described earlier in the "Static Aeroelasticity" section. One can see that predicted critical speeds are close to test results.

Experimental values of flutter frequency in all tests were 1.1–1.2 Hz. Theoretical results in the case of varying angle of attack are

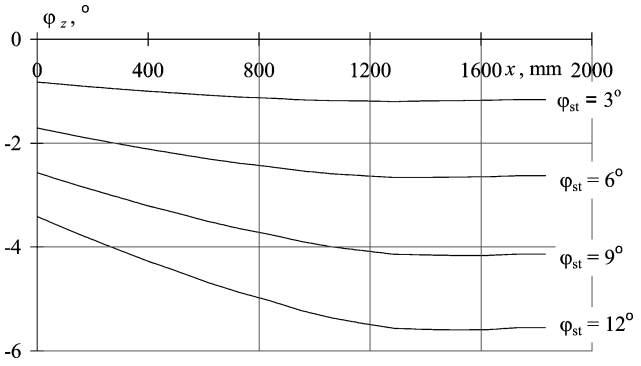


**Fig. 3 Spanwise distribution of elastic rotation angles $\varphi_z$ for flow sections of stabilizer at various stabilizer setting angles; flow velocity 25.5 m/s.**

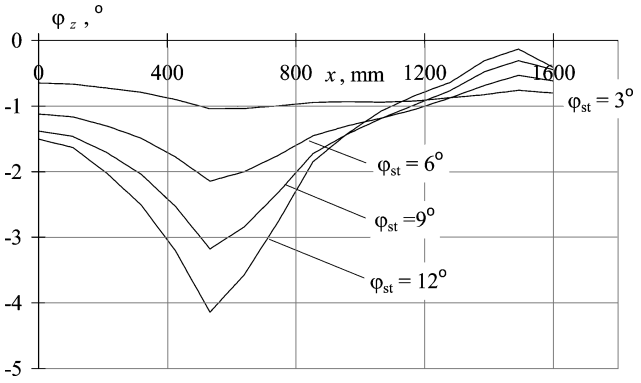


**Fig. 4 Spanwise distribution of elastic rotation angles $\varphi_z$ of flow sections of elevator at various stabilizer setting angles; flow velocity 25.5 m/s. Station 530 mm corresponds to elevator actuator.**

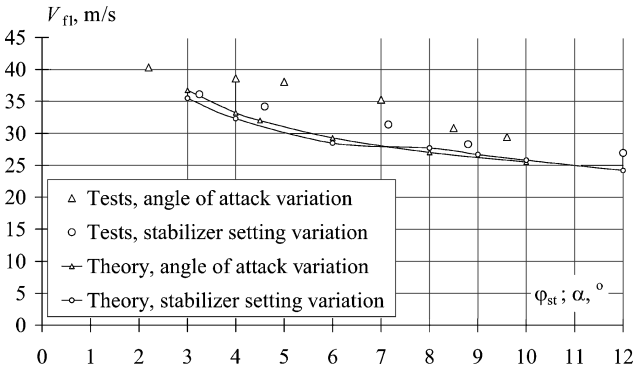


**Fig. 5 Flutter critical speed as a function of angle of attack and stabilizer setting: initial geometry.**

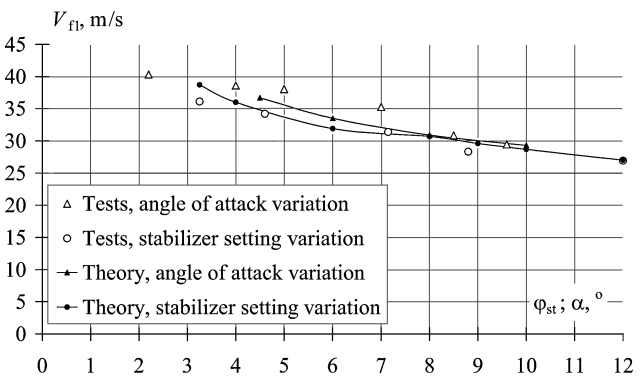


**Fig. 6 Flutter critical speed as a function of angle of attack and stabilizer setting: deformed geometry.**

1.6–1.67 Hz, whereas in the case of varying stabilizer setting angle, results were 1.35–1.45 Hz.

## Conclusions

One may conclude that the functional dependence of the critical speed on angle of attack and angle of stabilizer deflection is predicted precisely. This means that the supposition of 1) the significant influence of stabilizer in-plane oscillations and (2) the role of induced drag forces on the critical speed of flutter was absolutely right. Numerical results also demonstrate the significant influence of aeroelastic deformations due to angle of attack and the stabilizer deflection angle on critical parameters of flutter.

The convergence of critical frequencies is not as good. Averaged differences of frequencies are 0.25 Hz (when the stabilizer deflection is variable) and 0.45 Hz (when angle of attack is variable). This gives 22 and 39% deviations.

Reasons for the discrepancy are unknown. At least two causes may be assumed.

1) The numerical method uses quasi-steady aerodynamics, although flutter takes place at a rather large Strouhal number of 0.15–0.2;

2) There occurs restriction of rotational and torsional deformation of elevators due to the elevator rotation axis becoming curved within the elastic structure.

It is generally known that the flutter frequency is a more sensitive parameter, and its accuracy normally is worse than the accuracy of the critical speed. The author hopes that the situation may become better if the method is used with unsteady aerodynamics.

## Acknowledgments

The author is greatful to B.J. Chudayev for his efforts to restore all data on the dynamically similar model and tests (in which he participated as long ago as 1967–1970) as well as very useful in discussious of the present paper.

## References

[1]McCue, D. J., Gray, R., and Drane, D. A., "The Effect of Steady Tailplane Lift on the Subcritical Response of a Subsonic T-tail Flutter Model," Royal Aircraft Establishment R & M 3652, Farnborough, England, U.K., 1971.

[2]Hedman, S. G., "Vortex Lattice Method for Calculation of Quasi Steady State Loading on Thin Elastic Wing," Aeronautical Research Inst. of Sweden, Rept. 105, Sweden, Oct. 1965.

[3]Miranda, L. R., Elliott, R. D., and Baker, W.M., "A Generalized Vortex Lattice Method for Subsonic and Supersonic Flow Applications," NASA Langley Research Center, Rept. 2865, 1977.

[4]Albano, E., and Rodden, W. P., "Doublet-Lattice Method for Calculating Lift Distribution on Oscillating Surfaces in Subsonic Flow," *AIAA Journal*, Vol. 7, No. 2, 1969.

[5]Chuban, V. D., Ivanteyev, V. I., Chudayev, B. J., Avdeyev, E. P., and Shvilkin, V. A., "Numerical Simulation of Flutter Validated by Flight-Test Data for TU-204 Aircraft," *Computers and Structures*, Vol. 80, 2002, pp. 2551–2563.